Multivariate evaluation of the printing process on 3D printing of rice protein

Yeison Fernando Barrios-Rodríguez, Marta Igual, Javier Martínez-Monzó, Purificación García-Segovia[*]

i-FOOD, Instituto Universitario de Ingeniería de Alimentos-FoodUPV, Universitat Politècnica de València, Spain

A B S T R A C T

The combination of printing parameters appropriately improves the printability of 3D-printed foods. In this regard, the present study aims to evaluate the effect of 3D printing process parameters on protein food generation. Printability of a cylinder 3 cm in diameter and 1 cm in height using a protein mixture of rice water and xanthan gum with a ratio of 30:70:0.5 was evaluated in an extrusion printer with an XYZ system. A ½ fractional factorial design was used with three factors: nozzle diameter (1.2 – 2.2 mm), layer height (1.0 – 2.0 mm), and print speed (20 – 50 mm/s). Each combination of factor levels was performed in triplicate for 12 runs plus three central points. Print time (min), sample weight, change in diameter (%), change in height (%), change in volume (%), mass flow rate (mg/s), appreciation (qualitative variable), and textural and rheology characters were obtained as response variables. The linear effects of the factors and combination factors were evaluated by analysis of variance. Additionally, a principal component analysis was performed to visualize the similarity between the observations and the relationship between the variables. The results showed that the layer height and nozzle diameter affect the printing accuracy concerning surface quality, shape stability, resolution, and layer layout. The nozzle with a diameter of 1.7 mm combined with speeds between 35 and 50 mm/s allowed the effects of overextrusion to be overcome, generating a better flow of the material. Low scores in the printability variable were related to low-speed values (20 mm/s) and a high nozzle diameter (2.2 mm), which generated higher deformations in the printed protein cylinder. Additionally, some printing conditions affected the textural and rheological characteristics, which allowed inferring that the capacity of the protein mass to store and recover energy in compression processes is conditioned by the printing parameters.

1. Introduction

Food 3D printing is one of the most promising and innovative techniques in the food industry. Over time, this technology has undergone a fascinating evolution, giving rise to several revolutionary applications in gastronomy, personalized nutrition, and the creation of cutting-edge ingredients (Demei et al., 2022). However, its impact on food engineering is currently limited because it is a technique that involves crucial pre- and post-processing factors (Portanguen et al., 2021). These factors can be classified as i) extrusion mechanism, ii) material properties (rheological properties, textural properties, melting, glass transition), iii) processing factors (nozzle height, nozzle diameter, extrusion speed), and iv) post-processing treatments (Liu et al., 2017). In this regard, for developing suitable food 3D printing processes, the focus has been mainly on the rheological or textural characteristics of the printing inks (Dankar et al., 2018; Derossi et al., 2020; Fan et al., 2022). For example, proteins have been considered an important raw component for printing ink because of their shear-thinning behavior and fast recovery properties (Guo et al., 2022). Additionally, proteins such as rice protein provide essential amino acids that are lacking in other proteins such as methionine and cysteine; in addition, they have a mild flavor and are hypoallergenic and hypocholesterolemic (Agboola et al., 2005; Lee et al., 2022; Qiu et al., 2023). It has also been suggested that 3D-printed structures can withstand further processing by controlling the printing inks' physicochemical, rheological, structural, and mechanical properties (Godoi et al., 2016).

However, for more effective printing, the food's properties and the external components to which the printing inks are subjected need thorough consideration and analysis (Zhang et al., 2022). Processing parameters, such as nozzle diameter, layer height, extrusion rate, and

nozzle movement speed, are critical to print quality (Hao et al., 2010). 3D printing of fish surimi showed that applying a nozzle diameter between 0.8 mm and 1.5 mm generates inconsistent filaments. In contrast, using a larger nozzle diameter could extrude consistent lines, but the resolution and accuracy of the objects were poor (L. Wang et al., 2018). It has also been reported that layer height can be closely related to printing accuracy (Wu, 2018). The combination of appropriate shape parameters, such as nozzle diameter (1 mm), extrusion speed (24 mm 3/ s), and nozzle movement speed (30 mm/s), have proven to be optimal parameters for good lemon juice gel impression (Yang et al., 2018).

In this sense, the present study aims to evaluate the effect of 3D printing process parameters on the generation of protein foods. It is considered a fundamental hypothesis of the experiment that the variation of the printing parameters, such as layer height, print speed, and nozzle diameter, would significantly influence, independently and in their respective combinations, the process variables, food printability, textural, and rheological characteristics.

2. Methodology

2.1. Protein ink preparation

An 85 % rice protein isolate (Rice I850XF, Roquette Freres, France) with a particle size of 35–50 μm and a density of 0.400–0.450 kg/L was used. A mixture of 30 % rice protein, and 70 % water was prepared. A 0.5 % xanthan gum (Sosa Ingredients S.L, Barcelona, Spain) was added on this mixture basis. The percentage of hydrocolloids was selected according to the ranges reported in other works (Liu et al., 2019; Phuhongsung et al., 2020). The water was heated to 30 °C in a heating magnetic stirrer (VWR VMS-C7, Germany), and the xanthan gum was added, stirring until completely dissolved. It was then mixed with the rice protein, and before the printing, the mixture was tempered at 25 °C.

2.2. Experimental design

To evaluate the rice protein printing process, a ½ fractional factorial design (2^{p-k}) was performed with three experimental factors: i) A: layer height (1 mm − 2 mm), ii) B: print speed (20 mm/s − 50 mm/s), and iii) C: nozzle diameter (1.2 mm − 2.2 mm). The layer height was the exact height of each extruded material layer, print speed was the speed at which the head moved on each axis, and the nozzle diameter was the last step through which the food ink was extruded.

The tests were performed in three independent blocks (each block is an experimental replicate), one central point per block, with 15 experimental runs performed, considering three replicates per experimental condition(Table 1). The generator of the design was set as "C = AB," which implies a unique combination of factors A and B to obtain factor C and block generators were based on the concept of replicas. The observed alias structures or combinations of factors affecting the response variables were as follows: I + ABC, A + BC, B + AC, and C + AB. These combinations indicate that specific main effects may be indistinguishable from interactions between factors.

2.3. Extrusion 3D printing

A commercial 3D printer (More 2 Pro 3D, Shenzhen Technology Co, China) was used for printing rice protein, with a precise X-Y-Z positioning system and an extrusion system controlled by stepper motors. The 3D printing system was fed from a plunger with a piston connected to a worm screw. Printing assays were carried out at room temperature (temperature = 25.1 ± 0.3 °C and HR = 51 ± 2 %) with a protein mixture of 250 g per experimental block. A cylinder (3 cm in diameter and 1 cm in height, with a range of layer number of 5 to 10) was designed using Thinkercad (Thinkercad, free software, Autodesk, Inc., San Rafael, CA, USA) (Fig. 1). Once the figure is modeled, the Cura Ultimaker (version 5.1.1 developed by Ultimaker B.V) will configure the
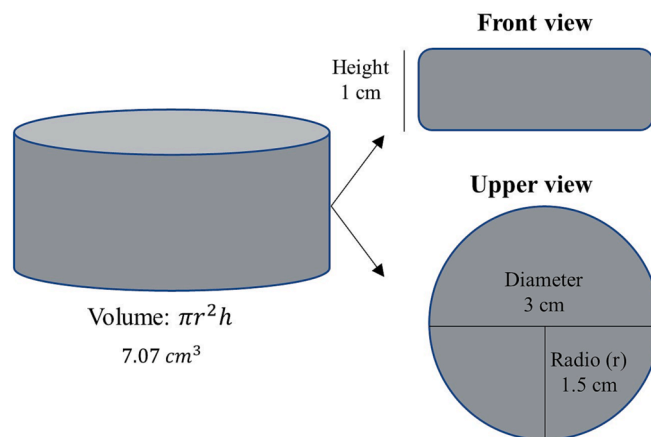
Table 1
A ½ fractional factorial design (2^{p-k}) for 3D printing process parameters.

n	Block	Code			Actual			Treatment*
		A	B	C	A	B	C	
1	1	−1	−1	1	1	20	2.2	A1:B20:C2.2
2	1	1	1	1	2	50	2.2	A2:B50:C2.2
3	1	1	−1	−1	2	20	1.2	A2:B20:C1.2
4	1	−1	1	−1	1	50	1.2	A1:B50:C1.2
5	1	0	0	0	1.5	35	1.7	A1.5:B35:C1.7
6	2	−1	1	−1	1	50	1.2	A1:B50:C1.2
7	2	1	−1	−1	2	20	1.2	A2:B20:C1.2
8	2	−1	−1	1	1	20	2.2	A1:B20:C2.2
9	2	1	1	1	2	50	2.2	A2:B50:C2.2
10	2	0	0	0	1.5	35	1.7	A1.5:B35:C1.7
11	3	−1	1	−1	1	50	1.2	A1:B50:C1.2
12	3	1	1	1	2	50	2.2	A2:B50:C2.2
13	3	1	−1	−1	2	20	1.2	A2:B20:C1.2
14	3	−1	−1	1	1	20	2.2	A1:B20:C2.2
15	3	0	0	0	1.5	35	1.7	A1.5:B35:C1.7

A: layer height (mm); B: print speed (mm/s); C: nozzle diameter (mm).
*Treatment was defined as the combination of the factors layer height (A), printing speed (B), nozzle diameter (C). This information was used for multivariate analysis.

Fig. 1. Cylinder design with Thinkercad for rice protein 3D printing.

printing parameters, as explained in Table 1. Additionally, the section parameters of layer height (initial layer height, line width, wall line width, infill line width, infill line width) and print speed (infill speed, wall speed, travel speed, initial layer speed, skirt/brim speed) were set to the corresponding values in Table 1 for each experiment for layer height and print speed. Infill density was 80 %, and infill patron was of lines.

2.4. Process parameters

During the print process, the time of each test in minutes and the weight of each cylinder in grams were determined with an analytical and precision scale (Ohaus, model PA2202C, Switzerland). The printed figure mass flow in mg/s was also calculated by dividing the total mass in grams by the real printing time in seconds. Additionally, the apparent density (ρ_b) was determined before and after printing according to the following equation (1):

$$\rho_b = \frac{m_s}{v_s} \tag{1}$$

Where ρ_b is apparent density in g/mL, m_s is the weight of the sample in g, and vs is the volume of the sample in mL, respectively. For this, 4 mL of the printed protein mass was placed in a graduated cylinder and weighed on a precision scale (Ohaus, model PA2202C, Switzerland) to

determine its mass. Two density measurements were performed for each experimental trial, as described in Table 1.

2.5. Shape change

Images of the top and side view of each freshly printed protein cylinder were taken with a quad camera with 48 MP AI of a Redmi Note 8 Edition cell phone (Xiaomi Inc., Beijing, China). The camera was always adjusted to the same distance using a tripod to take each image. To determine shape parameters, these images were processed in ImageJ software (ImageJ, NIH, Washington, DC, USA). After calibration, five height and diameter measurements were taken for each image of the printed protein cylinder. The diameter of the cylinder's base was measured in the upper view images, and the height was measured in the front view images (Fig. 1). The differences between the geometrical characteristics of the designed cylinder and the printed one were calculated as percent variation for each dimension according to the following equation (2):

$$\%change = 100 - \frac{A1}{A2}*100 \qquad (2)$$

Where A1 is the geometric characteristic measured on the printed protein cylinder (diameter, height, volume) in millimeters, and A2 is the programmed geometric characteristic (diameter, height, volume) in millimeters.

In addition, to appreciate the desired print quality, a subjective variable called appreciation was evaluated on a range of 0 to 5, with 0 being a print with poor shape characteristics and 5 being a print with good shape characteristics.

2.6. Rheological analysis

Rheological parameters of rice protein masses before and after printing were determined in triplicate. A rheometer HAAKE RheoStress 1 (Thermo, Massachusetts, USA) equipped with a 60 mm diameter parallel-plate rough geometry with a 1.0 mm gap between plates to perform oscillatory tests on protein ink before and after print was used. Data acquisition and evaluation were carried out using RheoWin software (Thermo, Massachusetts, USA). The amplitude sweep test was used to determine the linear viscoelastic region for all samples. The initial shear stress varied from 0.1 % to 10 % at the end of the 1 Hz frequency. An oscillatory test was performed at a fixed strain of 1 Pa and a frequency range of 0.1 to 10 Hz at 25 °C. The values of elastic modulus (G'), storage modulus (G''), and complex viscosity (η) were obtained by this analysis.

2.7. Textural characterization

TPA was performed on protein cylinders after 3D printing using a TA. XT.plus texturometer (Stable Micro Systems, Godalming, Surrey, UK). The TPA was executed with a cylindrical aluminum probe (4 cm in diameter) using a 50 kg load cell. The texture analysis was performed with double compression with a speed of 0.5 mm/s, with a rest period of 5 s between cycles, and the deformation was 40 % of the original length. All tests were performed at room temperature (25 °C). The parameters hardness, adhesiveness, cohesiveness, springiness, gumminess, and resilience were extracted using the Texture Exponent 32 program (Stable Micro Systems, Godalming, Surrey, UK).

2.8. Statistical analysis

An analysis of variance with a confidence level of 95 % was performed to determine the individual and combined influence of the different factors (layer height, print speed, nozzle diameter) on each of the variables' response to process parameters, shape change, rheology, and textural characteristics. The repeatability of the print was checked

with the analysis of the combinate factors. The analysis included Fisher's least significant difference (LSD) post hoc comparisons to establish which mean values were statistically different at an alpha level 0.05. A principal components analysis (PCA) was then performed with all the variables to identify grouping patterns, given by the effect of the printing conditions. The contribution of each variable to each observation was obtained to identify which variables are driving the position of a particular observation in the score space. This was achieved by multiplying the score matrix by the transposed loadings matrix ($\overline{\overline{TP^T}}$). Finally, a Pearson correlation was performed to corroborate the associations of the associated variables in the principal component analysis. Statistical procedures were performed with the General Public License of the R Core Team software (R Core Team, 2022).

3. Results and discussion

3.1. Effect of printing process variables on printed protein characteristics

3.1.1. Process parameters

Density (0.82 to 0.94 kg/L) was the only variable not affected by the factors evaluated (layer height, print speed, nozzle diameter) (Table 2). Layer height and nozzle diameter significantly affected ($p < 0.05$) the mass weight, print time, and mass flow, while print speed evidenced only an effect on print time and mass flow (Table 2). In this sense, the 1 mm layer height evidenced higher print time averages (245.5 ± 90.6 s), while with the 2 mm layer height, greater printed mass weight (9.25 ± 2.1 g) and mass flow (90.5 ± 33.5 mg/s) were obtained. On the other hand, when analyzing the nozzle diameter as an independent factor, the highest values of mass weight (10.5 ± 0.8 g), print time (213 ± 53.9 s), and mass flow (75.15 ± 20.5 mg/s) were evident at a diameter of 2.2 mm. Since the experimental design used is a fractional factorial design, the main effects and double interactions are confounded with each other, which means that it is not feasible to attribute specific effects to dual interactions. However, it is possible to obtain indications of the influence of double interactions by analyzing the main effects and their relationship with the factors involved. Therefore, it is feasible to deduce that the interaction of print speed with layer height (confounded with the C: nozzle diameter effect) and the interaction of print speed with nozzle diameter (confused with the A: layer height effect) may have some additional impact that adds to the individual effect of nozzle diameter (C) and layer height (A), respectively, on the variables of sample weight, print time and mass flow. In the same way, the interaction of layer height and nozzle diameter, confounded with the effect of print speed (B), may have an additional impact on the time and mass flow variables. This demonstrates that these three factors and their interactions significantly affect printing behavior, which, as discussed below, impacts the ideal printability characteristics.

When evaluating the combination of all linear factors as treatments, it is observed that there are significant differences between printing conditions in the variables of sample weight, print time, mass flow, and density (Fig. 2). The shortest print times were obtained with A1.5:B35:C1.7 (layer = 1.5 mm, print speed = 35 mm/s, nozzle diameter = 1.7 mm) and the treatment A2:B50:C2.2 (layer = 2 mm, print speed = 50 mm/s, nozzle diameter = 2.2) with 98.6 ± 1.2 s and 92.3 ± 2.5 s, respectively (Fig. 2), which is due to the use of high speeds and layer heights. The deposited mass flow is crucial to know how much is required for a given figure, and it is evident that the process conditions affect this parameter, generating higher mass flow in short time conditions as described above (71.4 ± 3.6 mg/s and 120.9 ± 1.9 mg/s respectively). This may be due to the nozzle diameter and layer height used, which cause more material to be deposited in less time. This indicates that short times in the printing process may not necessarily represent a lower amount of material used; it will depend on the other associated conditions (Fig. 2). It also stands out from this analysis that treatments with high material flow generated overextension of the

Table 2
Summary of the effect of the factors (layer height, printing speed, nozzle diameter), confidence intervals (CI), and p-value for each of the response variables studied.

Variables	Layer height				Print speed				Nozzle diameter			
	Effect	95 % CI	T-value	P-value	Effect	95 % CI	T-value	P-value	Effect	95 % CI	T-value	P-value
Process parameters												
Sample weight (g)	1.52	0.45;1.06	5.75	0.00	−0.175	−0.39;0.21	−0.66	0.53	3.982	1.68;2.29	15.08	0.00
Print time (s)	−138.16	−70.44;67.72	−117.5	0.00	−103.16	−52.94; −50.23	−87.72	0.00	73.16	35.23;35.94	62.21	0.00
Mass flow (mg/s)	57.84	26.60;31.25	28.68	0.00	33.65	14.50;19.15	16.69	0.00	27.09	11.22;15.87	13.43	0.00
Density (Kg/L)	−0.003	−0.02; 0.017	−0.21	0.840	−0.0072	−0.023; 0.015	−0.43	0.680	−0.029	−0.03; 0.01	−1.31	0.227
Shape change												
Height change (%)	−3.16	−4.02; 0.86	−1.49	0.174	1.81	−1.54; 3.35	0.85	0.418	−4.77	−4.83; 0.06	−2.25	0.054
Diameter change (%)	−8.32	−7.55; −0.77	−2.83	0.022	−4.91	−5.85; 0.94	−1.67	0.134	−11.80	−9.29; −2.51	−4.01	0.004
Volume change (%)	−12.48	−9.13; −3.35	−4.97	0.001	−4.08	−4.93; 0.85	−1.63	0.143	−17.99	−11.89; 6.10	−7.17	0.000
Appreciation	0.083	−0.413; 0.496	0.21	0.838	1.250	0.170; 1.080	3.17	0.013	−1.583	−1.25; −0.34	−4.01	0.004
Rheology												
Ǵ(10 Hz) [Pa]	−16	−1500; 1484	−0,01	0,990	991	−996; 1988	0,77	0,466	−1361	−2172; 812	−1,05	0,324
Ǵ(10 Hz) [Pa]	702	−4; 706	2,28	0,052	572	−69; 641	1,86	0,101	−1251	−981; −270	−4,06	0,004
η (10 Hz) [Pa]	3,7	−21,6; 25,3	0,18	0,861	16,1	−15,4; 31,5	0,79	0,451	−24,5	−35,7; 11,2	−1,20	0,263
Texture												
Hardness (N)	−0.393	−0.615; 0.222	−1.08	0.311	−0.216	−0.527; 0.310	−0.60	0.568	−0.890	−0.86; −0.027	−2.45	0.040
Cohesiveness	0.0339	−0.024; 0.058	0.95	0.371	−0.0145	−0.048; 0.034	−0.41	0.696	0.1012	0.009; 0.091	2.83	0.022
Springiness	−0.0488	−0.106; 0.057	−0.69	0.512	0.0200	−0.072; 0.092	0.28	0.785	0.1064	−0.028; 0.14	1.50	0.173
Adhesiveness (N*s)	−0.86	−3.50; 2.65	−0.32	0.756	2.62	−1.77; 4.39	0.98	0.355	0.33	−2.91; 3.24	0.12	0.904
Gumminess (N)	−0.1161	−0.268; 0.152	−0.64	0.542	−0.1920	−0.306; 0.114	−1.05	0.323	−0.1785	−0.299; 0.121	−0.98	0.356
Resilience	0.00489	−0.005; 0.010	0.74	0.481	0.00441	−0.005; 0.009	0.67	0.523	−0.0031	−0.009; 0.006	−0.47	0.652
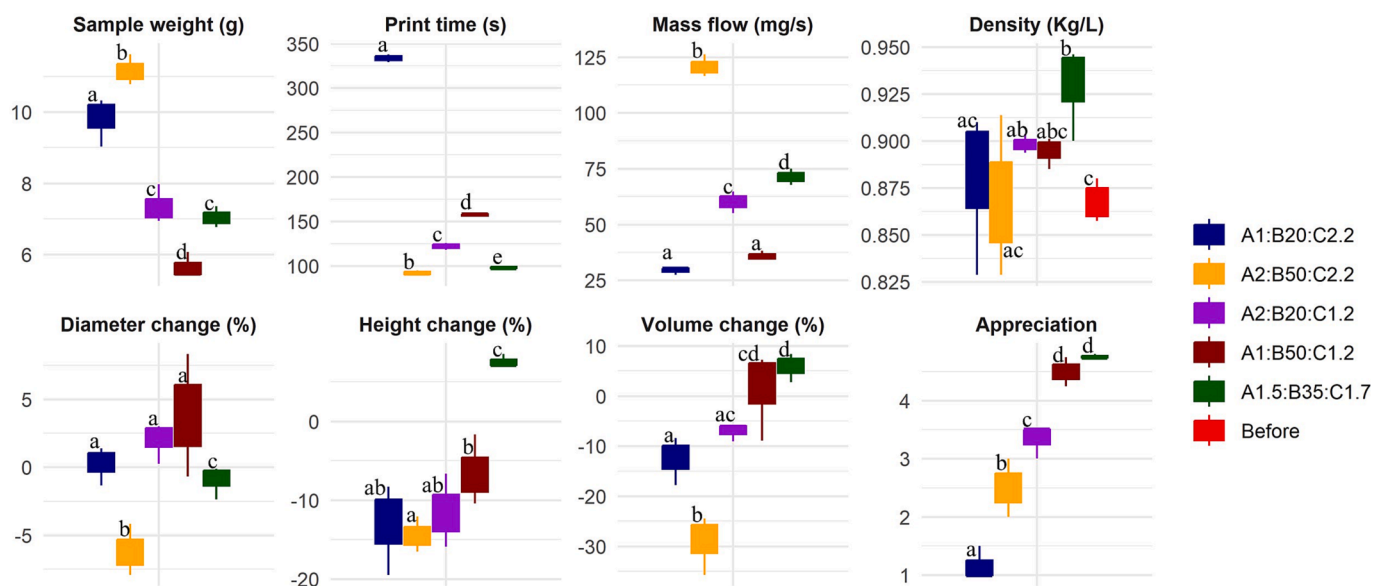
Fig. 2. The combined effect of the rice protein printing process factors on process and form characteristics. Different lowercase letters in boxes of the same variable indicate statistically significant differences (p < 0.05), n = 3. Where A is layer height (1, 1.5, or 2 mm), B is print speed (20, 35, or 50 mm/s), and C is nozzle diameter (1.2, 1.7, or 2.2 mm).
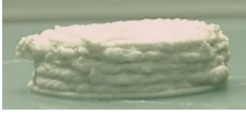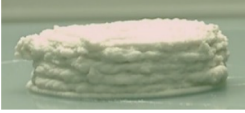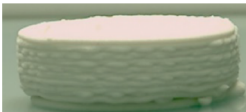
protein, exhibiting greater thickness, which may result in a low-resolution printed structure (Phuhongsung et al., 2022). As evidenced in Table 3, the low-printed resolution treatments have the highest mass flow (Fig. 2). These high mass flow can also be associated with the wavy lines evidenced during the printing process in the A2:B20:C1.2 treatment (Yang et al., 2018), where possibly the low print speed (20 mm/s) and the use of a higher layer height (2 mm) than the nozzle diameter (1.2 mm) can also influence.
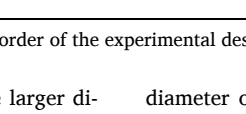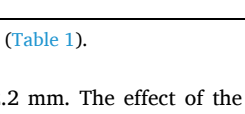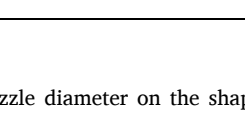
Finally, although density was not affected individually by the process parameters, the combination of the different parameters showed a significant effect (p < 0.05) before and after printing (Fig. 2). The differences may be because the mechanical forces to which the printing ink is subjected during the printing process may help to pack the protein mass better, given by the compression and compaction process in the protein extrusion before exiting through the nozzle. On the other hand, this same process can cause the air retained in the mass to be expelled, leaving less space and increasing the bulk density after printing (Fig. 2). As for the differences evidenced between A1.5:B35:C1.7 (layer height = 1.5, print speed = 35 mm/s, nozzle diameter = 1.7) with the A2:B50:C2.2 treatment (layer height = 2, print speed = 20 mm/s, nozzle

Table 3

Effect of printing parameters layer height, print speed, and nozzle diameter on rice protein printability.

Treatment	A: Layer height (mm)	B: Print speed (mm/s)	C: Nozzle diameter (mm)	Number of layers	Block 1	Block 2	Block 3
A1:B20: C2.2	1	20	2.2	10	1	8	14
A2:B50: C2.2	2	50	2.2	5	2	9	12
A2:B20: C1.2	2	20	1.2	5	3	7	13
A1:B50: C1.2	1	20	1.2	10	4	6	11
A1.5:B35: C1.7	1.5	35	1.7	7	5	10	15

The numbers below each experimental image indicate the running order of the experimental design (Table 1).

diameter = 2.2), they can be attributed to the fact that the larger diameters are those that generate more minor pressure changes in the system, therefore less compaction and expulsion of air from the protein mass.

3.1.2. Shape change

The analysis of individual effects showed that print speed did not significantly affect (p > 0.05) any of the shape change variables (Table 2). The layer height showed a significant effect (p < 0.05) on the diameter change and volume change obtained from the printed cylinder (Table 2). In the change of diameter, it was found that layer height of 1 mm decreased the programmed diameter (2.3 ± 1.4 %), while layer heights of 2 mm exceeded the diameter limit of 3 cm programmed for printing (2.1 ± 1.9 %). Nozzle diameter had significant effects (p < 0.05) on each of the variables associated with changes in shape (height change [%], diameter change [%], volume change [%], and appreciation). In this case, the most considerable diameter changes (2.9 ± 1.5 %), height changes (13.77 ± 1.6), volume change (20.7 ± 4.2), and the lowest appreciation value (1.8 ± 0.3) were evident with a nozzle

diameter of 2.2 mm. The effect of the nozzle diameter on the shape characteristics ultimately impacts the appreciation. The increase in nozzle diameter causes the impression to become more extensive due to the high mass flow described above, leading to lower impression accuracy and, as a result, inadequate weight distribution (Pérez et al., 2019; Yang et al., 2017). The nozzle diameter is essential to establish good print quality and ensure the layers overlap correctly (Dankar et al., 2018). The results corroborate that the layer height and nozzle diameter affect the printing precision regarding surface quality, shape stability, resolution, discontinuous printing lines, and extrusion, as evidenced in other studies (Hao et al., 2010; Keerthana et al., 2020). It is evident that under these experimental conditions, the nozzle with a diameter of 1.7 mm allows a continuous and uniform flow of the material supply, which, combined with speeds between 35 and 50 mm/s, could overcome the effects of over-extrusion.

As in the previous analysis, it is possible to intuit that the interactions of layer height with print speed (confounded by the C-effect) may have an additional effect on all shape change variables. It has been evidenced that print speed has a considerable impact on the growth kinetics of

printed food height (Derossi et al., 2018), which may help to corroborate the synergistic effect of print speed and layer height on shape characteristics. When analyzing the combinations of the different parameters, it is evident that there are only significant differences in the height change in A1.5:B35:C1.7 (layer height = 1.5 mm, print speed = 35 mm/s, nozzle diameter = 1.7 mm) [9.9 ± 4.8 %], showing a positive percentage (Fig. 2), which indicates that, unlike the other treatments, the height values were lower than those of the figure programmed in the Thinkercad. Regarding the change in diameter, the only treatment that presented significant differences (p < 0.05), with a value of −6.2 ± 1.9 %, was A2:B50:C2.2 (layer height = 2 mm, print speed = 50 mm/s, nozzle diameter = 2.2), being the same treatment that presented the highest mass flow, originated by a short print time and high sample weight. It is possible that these conditions led this treatment to one of the lowest scores on the appreciation variable (2.5 ± 0.5), along with treatment A1:B20:C2.2 (layer height = 1 mm, print speed = 20 mm/s, nozzle diameter = 2.2 mm) which obtained a value of 1.2 ± 0.3 (Fig. 2). The low scores in the appreciation variable were related to low-speed values (20 mm/s) and a high nozzle diameter (2.2 mm), which generated higher deformations in the printed protein cylinder, as evidenced in Table 3 and Fig. 2. This may be related to the fact that too low print speed causes material overflow, resulting in poor dimensional resolution of a printed object (Phuhongsung et al., 2022). On the contrary, the combinations made at the central point's A1.5:B35:C1.7 (layer height = 1.5 mm, print speed = 35 mm/s, nozzle diameter = 1.7 mm), as well as treatments with a low layer height (1 mm) and nozzle diameter (1.2 mm) at high speed (50 mm/s), allowing for a better definition and structure of the printed cylinder (Table 3).

3.1.2.1. Rheology and textural characterization. The analysis did not show significant effects (p < 0.05) for the layer height and print speed factors on any of the rheology and texture variables of printed samples (Table 2). However, the nozzle diameter factor shows significant effects on hardness and cohesiveness. In comparison to diameters of 1.2 and 1.7, the diameters of 2.2 mm presented lower hardness values (2.47 ± 0.66 N), while cohesiveness was lower with a nozzle diameter of 1.2 mm (0.47 ± 0.08). This indicates that this parameter affects the stress necessary to deform the protein cylinders after printing. In this case, the treatments with diameters of 2.2 mm did not present a homogeneous arrangement of the protein mass, showing damage in their geometry

(Table 3), which may explain why they decreased their hardness. Similarly, it may affect the mechanical strength of the internal bond of the cylinder and its resistance, generating an increase or decrease in cohesiveness (Ozel & Oztop, 2022). For example, tests with a nozzle diameter of 1.2 mm may present better internal bonding, developing a better geometrical structure of the printed protein cylinders, as evidenced in Table 3. This is because cohesion contributes to the material's ability to maintain continuity during 3D printing and cohesion of subsequent deposition layers (Wang et al., 2023). Also, the nozzle diameter may influence the pressure changes in the printing system, changing the microstructure of the printed masses and significantly affecting mechanical properties such as hardness and cohesion (Derossi et al., 2020). As for the combination of the process parameters, differences in hardness and gumminess were evidenced, with the lowest values for both in A2:B50:C2.2 (Fig. 3). It should be noted that gumminess is representative of the energy required to disintegrate a semisolid food by the mouth's structures (Chatzitaki et al., 2022) and is the result of hardness by cohesiveness. These results indicate that printing conditions can decrease or increase the mechanical requirements during consumption, which can be critical when designing foods for specific consumers.

As for the variables associated with rheology, only an effect of the nozzle diameter in G'' was evidenced, obtaining a lower value for the printed cylinder with a diameter of 2 mm (5533 ± 313 Pa). In this sense, it can be observed that a larger diameter decreases the liquid-viscous behavior in which energy dissipation occurs in the rice protein mass. Given this, it is hypothesized that changes in diameter generate pressure changes in the printing system, increasing (with smaller diameters) or decreasing (with larger diameters) the shear stress during extrusion, which would mean a difference in the rheological characteristics of the material. This is because the conditions of the printing process influence the printed material's microstructure (Derossi et al., 2020).

When analyzing the rheological properties in the different printing combinations (Table 4), it was evident that A1.5:B35:C1.7 presents statistically significant differences (p < 0.05) in G' (26824 ± 563 Pa) and η (442 ± 10 Pa) with the A1:B20:C2.2 treatment (G'=23405 ± 1227 Pa and η = 380 ± 19 Pa). The latter treatment, with a layer height of 1 mm, print speed of 20 mm/s, and nozzle diameter of 2.2 mm, also showed the lowest G'' (4896 ± 96 Pa). This indicates that the combination of intermediate printing process parameters (layer height = 1.5 mm, print speed = 35 mm/s, nozzle diameter = 1.7 mm) generates an
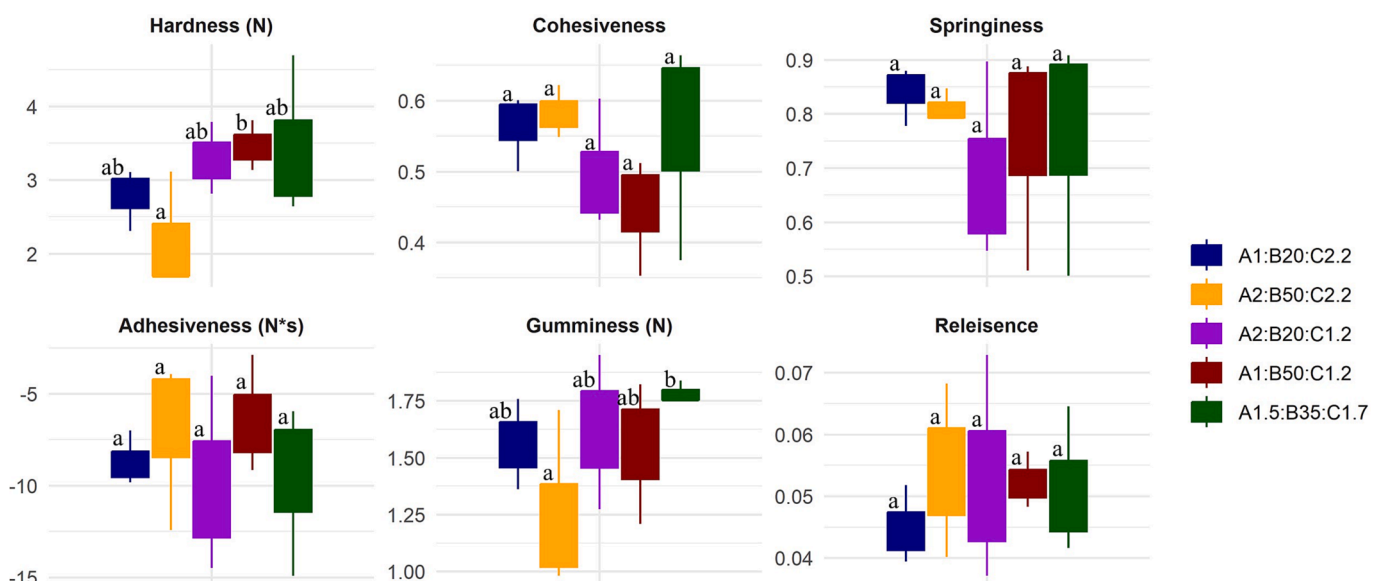

Fig. 3. The combined effect of printing process factors of printed rice protein on textural characteristics. Different lowercase letters in boxes of the same variable indicate statistically significant differences (p < 0.05), n = 3. Where A is layer height (1, 1.5, or 2 mm), B is print speed (20, 35, or 50 mm/s), and C is nozzle diameter (1.2, 1.7, or 2.2 mm).

Table 4
Rheological properties of proteins before and after printing at a frequency of 10 Hz. Where A is layer height (1, 1.5, or 2 mm), B is print speed (20, 35, or 50 mm/s), and C is nozzle diameter (1.2, 1.7, or 2.2 mm).

Treatment	G'[Pa]	G''[Pa]	η[Pa · s]
Before printing	23834 ± 346^{ab}	6175 ± 246^{b}	405 ± 3^{ab}
A1:B20:C2.2	23405 ± 1227^{a}	4896 ± 96^{a}	380 ± 19^{a}
A2:B50:C2.2	24380 ± 1203^{ab}	6170 ± 275^{b}	400 ± 18^{ab}
A2:B20:C1.2	24750 ± 1681^{ab}	6849 ± 241^{bc}	408 ± 26^{ab}
A1:B50:C1.2	25757 ± 980^{ab}	6719 ± 207^{bc}	421 ± 16^{ab}
A1.5:B35:C1.7	26824 ± 563^{b}	7264 ± 488^{c}	442 ± 10^{b}

Values are presented as mean ± standard error. Different lowercase letters in the same column indicate significant differences (p < 0.05) between treatments.

increase in elastic capacity and storage modulus concerning the masses printed under extreme conditions experienced in A1:B20:C2.2. The poor compaction and alignment of the layers observed in the printed protein cylinder in A1:B20:C2.2 (Table 3) may be due to these weaker mechanical strength characteristics (Cai et al., 2022). Additionally, the A1:B20:C2.2 print also presented significant differences (p < 0.05) in G''

with the mass before printing, showing lower storage modulus values (6175 ± 246 Pa). The A1.5:B35:C1.7 treatment, compared to the protein mass before printing, evidenced a significant increase in the storage modulus (7264 ± 488 Pa). In this sense, it can be inferred that some printing conditions affect the ability of the protein mass to store and recover energy in compression processes. In the case of A1:B20:C2.2, it is possible that in addition to alterations in the geometry of the printed object that decrease the hardness, as discussed above, hydrogen bond interactions, ionic interactions, and van der Waals forces, which contribute to stability and stiffness (Karshikoff et al., 2015), could weaken or broken due to stress conditions. However, under other working conditions, such as those performed in A1.5:B35:C1.7, the dough could undergo a structural reorganization that would improve its rheological characteristics.

The above results show that although rheological parameters help formulate food 3D printing materials, they cannot fully describe the printing process's complexity (Fan et al., 2022). Viscosity (η) and the storage (G') and loss (G'') modules provide essential information about the flow properties and mechanical response of materials (Fan et al., 2022); however, they do not capture all relevant aspects of the food 3D
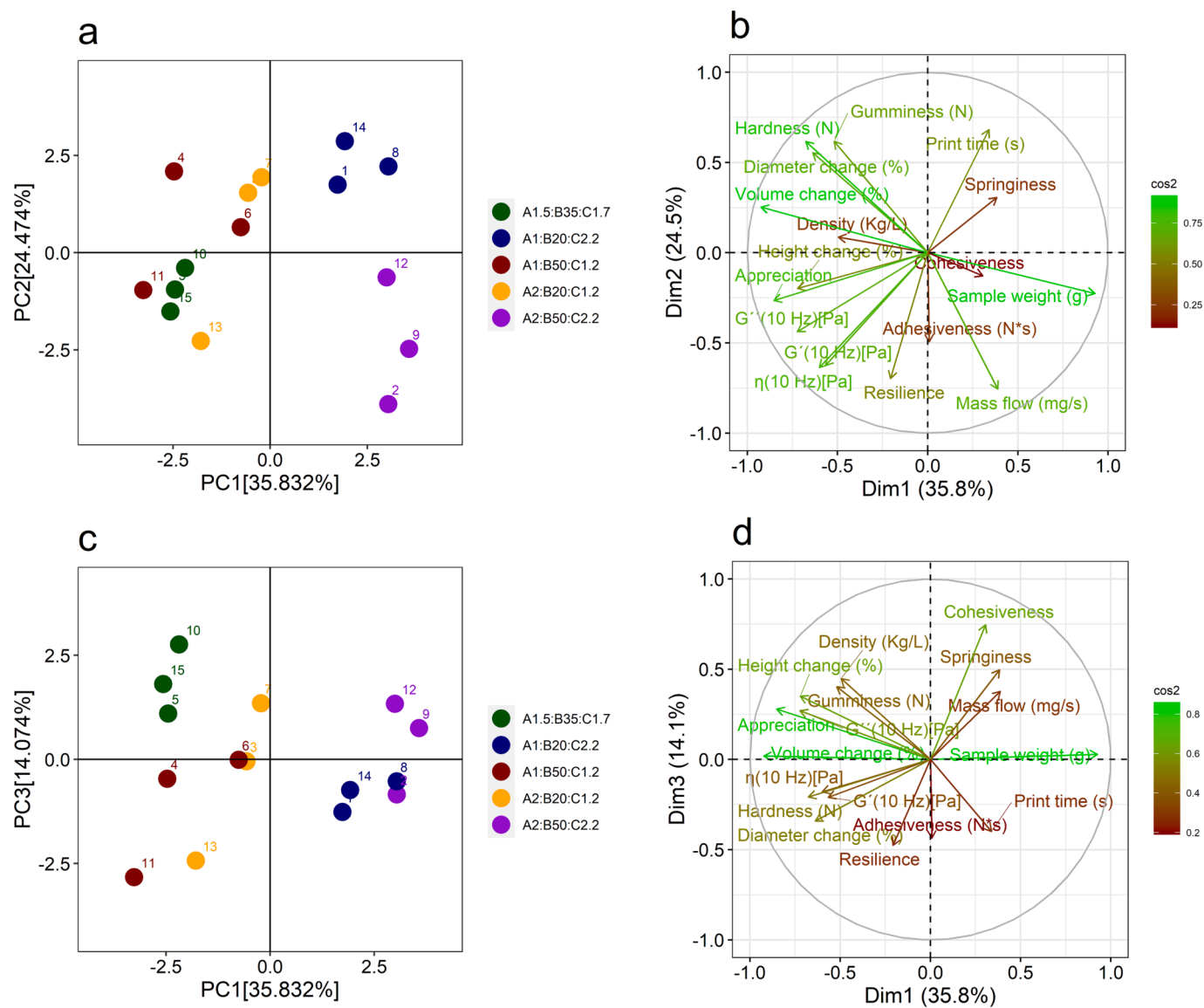
Fig. 4. Grouping of observations by the effect of printing conditions obtained by PC1 VS PC2 (a), PC1 VS PC3 (c), and contribution of each variable to the data structure in PC1 VS PC2 (b) and PC1 VS PC3 (d). Where A is layer height (1, 1.5, or 2 mm), B is print speed (20, 35, or 50 mm/s), and C is nozzle diameter (1.2, 1.7, or 2.2 mm).

printing process. As shown in the results, an adequate adjustment of the printing parameters is necessary to guarantee an ideal printing process and reduce the effect on the mechanical characteristics of the printed food.

3.2. Processing grouping according to printing conditions

The multivariate analysis allowed us to infer that some of the evaluated treatments showed similarities. The score plot with the first two components (Fig. 4a) shows clustering patterns of treatments A1.5:B35:C1.7 mainly along the negative part of PC1 (36.45 %) in the quadrant IV of the Cartesian square. Treatments A1:B20:C2.2 (layer height = 1 mm, print speed = 20 mm/s, nozzle diameter = 2.2 mm) and A2:B50:C2.2 (layer height = 2 mm, print speed = 50 mm/s, nozzle diameter = 2.2 mm) were grouped in the positive part of CP1, in quadrant I and IV, respectively. Although this graph was not conclusive for all treatments, specifically for A1:B50:C1.22 and A2:B20:C1.2, when plotting PC1 vs. PC3, it corroborated the above observations' clustering (Fig. 4c) and evidenced the possible similarity in print quality in the treatment samples A1:B50:C1.22 and A2:B20:C1.2. This shows that PC3 (13.81 %) is capturing characteristics or patterns of variability of information that are not captured by PC2 (23.6 %). This clustering pattern is due to the variability in the different aspects (shape, textural, rheological) caused by the combination of the different printing process parameters.

The loadings plot of the variables allowed inferring that samples A1.5:B35:C1.7 owe their spatial distribution to higher values in the appreciation variable, G'' at 10 Hz and height change (Fig. 4b-d); this treatment was considered as the one with the best printability characteristics (Table 3). On the other hand, A1:B20:C2.2 and A2:B50:C2.2 were located on the opposite side; A1:B20:C2.2 was related to higher printed mass weight and longer printing times, while cohesiveness and springiness were more related to the A2:B50:C2.2 treatment (Fig. 3d). It is highlighted that the treatments A1:B20:C2.2 and A2:B50:C2.2 negatively correlate with the variable appreciation, hardness, and rheological characteristics. This explains these conditions' drawbacks to obtaining adequate printability characteristics (Table 3).

In addition, to understand the behavior of treatments A1:B50:C1.2 and A2:B20:C1.2, the contribution of each variable to each of the observations was established (Fig. 5). These treatments presented more heterogeneous distributions because some variables presented higher or lower contributions. For example, in observation 13 of treatment A2:B20:C1.2, higher contributions were found for variables such as sample weight and volume change, as well as contributions with an opposite sign concerning their replicates in variables such as mass flow, diameter change, G' at 10 Hz, hardness, cohesiveness, springiness, and resilience (Fig. 5a). As for treatment A1:B50:C1.2 for observation 11, more significant contributions from variables such as mass flow, diameter change, volume change, G', η at 10 Hz, and cohesiveness were observed (Fig. 5b). This shows how heterogeneous the printing process can be even under the same conditions. One explanation may be the pressure
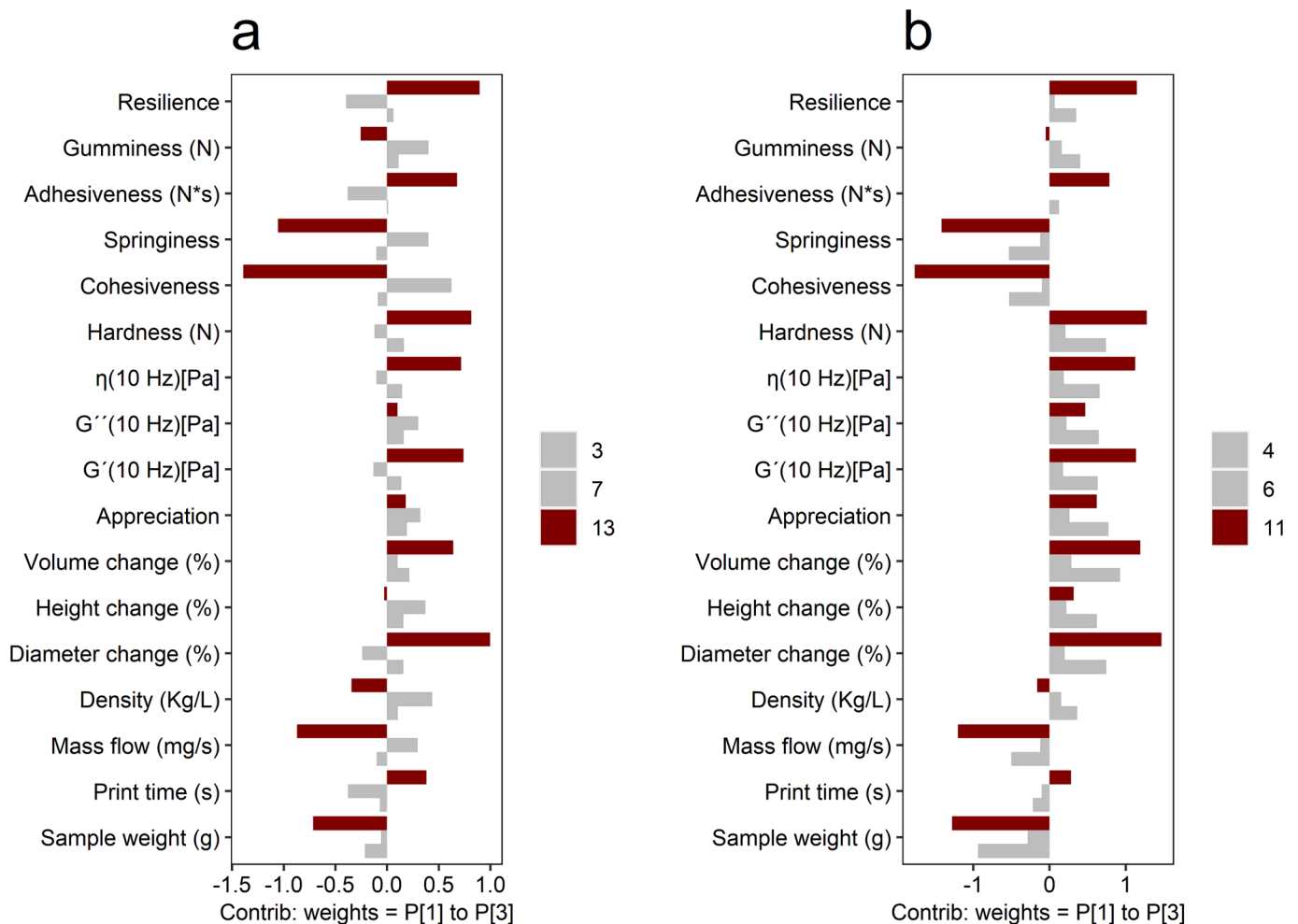

Fig. 5. Contribution of the variables to the observations 3,7, and 13 (defined in Table 1) of A2:B20:C1.2 (layer height = 2 mm, print speed = 20 mm/s, and nozzle diameter = 1.2 mm) (a) and the observations 4, 6, and 11 (defined in table 1) of A1:B50:C1.2 (layer height = 1 mm, print speed = 50 mm/s, and nozzle diameter = 1.2 mm) (b), obtained through CP1 and CP3.

gains or losses due to the constant change in diameter caused by the process. As discussed above, during printing, when a viscoelastic material is subjected to forced flow through cylinders of different diameters, the resistance to flow can vary. As the material passes through cylinders of different diameters, it may undergo elastic and viscous deformation, resulting in pressure changes as it conforms to the other cylinder diameters.

The loadings plot also showed that some variables may be highly correlated (Fig. 4b-d), such as the appreciation variable with G'' at 10 Hz or hardness with G' at 10 Hz. These relationships were corroborated by Pearson's correlation with their respective significance (Fig. 6). The correlations of the variable appreciation with sample weight (-0.8***) and print time (-0.7***) stand out. This indicates that it is necessary to develop processes with shorter print times to approximate a more adequate or acceptable print. As shown in Fig. 2, treatments A1:B20: C2.2 and A2:B50:C2.2 presented the highest mass values (9.8 ± 0.7 g and 11.2 ± 0.4 g), being A1:B20:C2.2 the one with the longest print time (157.3 s), these same treatments presented deformations in their geometric and definition characteristics during the printing process (Table 3).

The appreciation variable is closely linked to changes in the shape of the printed cylinder, evidenced by its highly positive correlations with volume change and height change (0.7**). As explained above, changes in cylinder geometric shapes are generated mainly by large nozzle diameters and, in addition to developing a low appreciation score, can also affect rheological and textural conditions, which explains the high correlation of G'' at 10 Hz (0.8***) with appreciation. On the other hand, sample weight also showed a negative correlation with hardness (-0.6*) and G'' at 10 Hz (-0.6*). This indicates that higher weights decrease these textural and rheological parameters, which, as discussed above, is due to the over-extrusion processes that generate poor positioning of printing layers, alterations in the geometry, and a decrease in the viscous liquid behavior of the protein mass. The above is further corroborated by the positive correlation of volume change with hardness (0.8***) and gumminess (0.5*), evidencing an effect of the change in geometric characteristics on the textural conditions of the printed protein. The positive correlation of volume change with hardness (0.8***) and gumminess (0.5*) further reinforces this statement. It evidences an effect of the geometrical change characteristics on the textural conditions of the printed protein. On the other hand, the negative correlation of time with G'' (-0.8***) indicates that long print times might not be adequate since they affect the rheological conditions of the material. Finally, the positive correlation of resilience with G' (0.6*) and η (0.6*) at 10 Hz is noteworthy, indicating that protein cylinders, as they increase their energy storage capacity and dynamic shear strength (by modifying the printing parameters), may be better able to recover their initial shape after deformation stress.
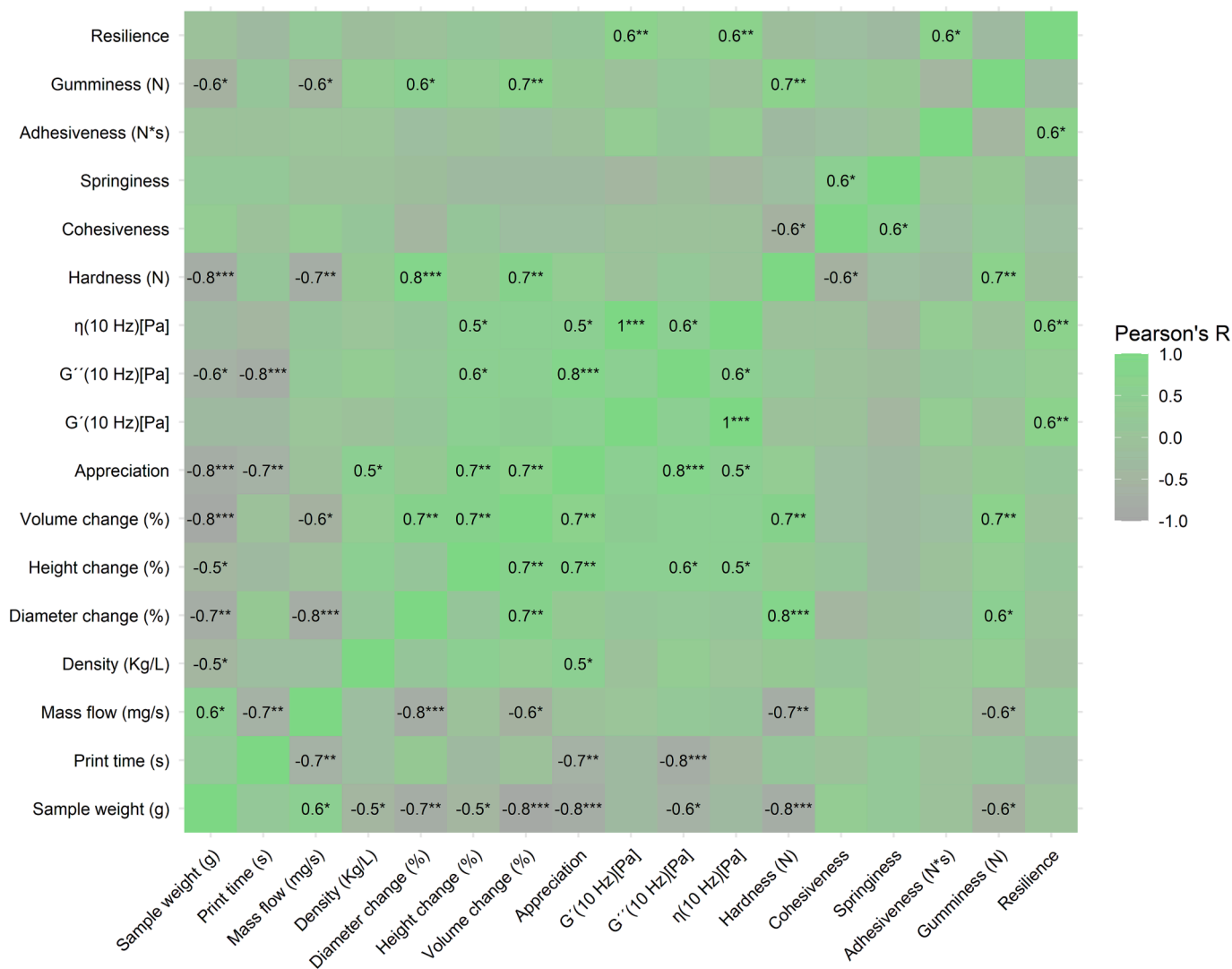

Fig. 6. Significance and direction of linear association between printing process, shape change, rheological and textural variables.

4. Conclusions

The printability of food is strongly conditioned by the printing parameters, as evidenced by the results obtained in this study. Most works adapt the masses to specific printing conditions, mainly generating ideal rheological conditions. However, it is possible that printing inks can be adjusted through proper management of parameters without relying too much on rheological characteristics. This work showed that a mass with specific mechanical characteristics can generate good or poor printing results, conditioned by the factors of the printing process. The layer height, print speed, and nozzle diameter significantly affect the surface quality print, shape stability, and resolution characteristics. A high diameter (2.2 mm) was the least recommended for rice protein printing processes. Under the experimental conditions, combining a nozzle with a layer height of 1.5 mm, diameter of 1.7 mm, and print speed between 35 and 50 mm/s could help decrease the effects of over-extrusion, allowing a continuous and uniform flow of the material supply. In addition, some conditions such as A1:B20:C2.2 (layer height 1 mm, velocity 20 mm/s, nozzle diameter 2.2 mm) with A1.5:B35:C1.7 (layer height 1.5 mm, velocity 35 mm/s, nozzle diameter 1.7 mm) differed significantly in variables such as elastic modulus, storage, complex viscosity, and bulk density. This was attributed to the mechanical forces to which the material is subjected during the printing process and the influence of the printing parameters to increase or decrease these mechanical forces. That is, depending on the conditions to which the printing inks are subjected, the ability of the protein mass to store and recover energy in compression processes is affected. Therefore, it is critical to consider these effects when developing printed protein foods. Finally, it is essential to establish ideal printing conditions for any type of dough, so it is necessary to advance in optimizing the influential parameters in this process, evaluating its effect on the final characteristics of the printed food.

CRediT authorship contribution statement

Yeison Fernando Barrios-Rodriguez: Writing – review, Conceptualization, Methodology, and Editing. **Marta Igual-Ramo:** Supervision, Methodology, and Revision of the final document. **Javier Martínez-Monzó:** Funding, Supervision, Methodology, Conceptualization, Language check, and Revision of the final document. **Purificación García-Segovia:** Funding, Supervision, Methodology, and Revision of the final document.

Declaration of competing interest

The authors declare that they have no known competing financial interests or personal relationships that could have appeared to influence the work reported in this paper.

Data availability

Data will be made available on request.

Acknowledgments

References

Agboola, S., Ng, D., & Mills, D. (2005). Characterisation and functional properties of Australian rice protein isolates. *Journal of Cereal Science, 41*(3), 283–290. https://doi.org/10.1016/j.jcs.2004.10.007

Cai, Q., Zhong, Y., Xu, M., Huang, Q., & Lu, X. (2022). 3D printed high oil custard cream: Effects of whey protein isolate, hydroxypropylated starch and carrageenan on physicochemical properties and printing performance. *LWT, 156*. https://doi.org/10.1016/j.lwt.2021.113039

Chatzitaki, A. T., Mystiridou, E., Bouropoulos, N., Ritzoulis, C., Karavasili, C., & Fatouros, D. G. (2022). Semi-solid extrusion 3D printing of starch-based soft dosage forms for the treatment of paediatric latent tuberculosis infection. *Journal of Pharmacy and Pharmacology, 74*(10), 1498–1506. https://doi.org/10.1093/jpp/rgab121

Dankar, I., Pujolà, M., El Omar, F., Sepulcre, F., & Haddarah, A. (2018). Impact of Mechanical and Microstructural Properties of Potato Puree-Food Additive Complexes on Extrusion-Based 3D Printing. *Food and Bioprocess Technology, 11*(11), 2021–2031. https://doi.org/10.1007/s11947-018-2159-5

Demei, K., Zhang, M., Phuhongsung, P., & Mujumdar, A. S. (2022). 3D food printing: Controlling characteristics and improving technological effect during food processing. In *Food Research International* (Vol. 156). Elsevier Ltd. 10.1016/j.foodres.2022.111120.

Derossi, A., Caporizzi, R., Azzollini, D., & Severini, C. (2018). Application of 3D printing for customized food. A case on the development of a fruit-based snack for children. *Journal of Food Engineering, 220*, 65–75. https://doi.org/10.1016/j.jfoodeng.2017.05.015

Derossi, A., Caporizzi, R., Oral, M. O., & Severini, C. (2020). Analyzing the effects of 3D printing process per se on the microstructure and mechanical properties of cereal food products. *Innovative Food Science and Emerging Technologies, 66*. https://doi.org/10.1016/j.ifset.2020.102531

Fan, F., Li, S., Huang, W., & Ding, J. (2022). Structural characterization and fluidness analysis of lactose/whey protein isolate composite hydrocolloids as printing materials for 3D printing. *Food Research International, 152*. https://doi.org/10.1016/j.foodres.2021.110908

Godoi, F. C., Prakash, S., & Bhandari, B. R. (2016). 3d printing technologies applied for food design: Status and prospects. In *Journal of Food Engineering* (Vol. 179, pp. 44–54). Elsevier Ltd. 10.1016/j.jfoodeng.2016.01.025.

Guo, Z., Arslan, M., Li, Z., Cen, S., Shi, J., Huang, X., … Zou, X. (2022). Application of Protein in Extrusion-Based 3D Food Printing: Current Status and Prospectus. *Foods, 11*(13), MDPI. https://doi.org/10.3390/foods11131902

Hao, L., Mellor, S., Seaman, O., Henderson, J., Sewell, N., & Sloan, M. (2010). Material characterisation and process development for chocolate additive layer manufacturing. *Virtual and Physical Prototyping, 5*(2), 57–64. https://doi.org/10.1080/17452751003753212

Karshikoff, A., Nilsson, L., & Ladenstein, R. (2015). Rigidity versus flexibility: The dilemma of understanding protein thermal stability. In *FEBS Journal* (Vol. 282, Issue 20, pp. 3899–3917). Blackwell Publishing Ltd. 10.1111/febs.13343.

Keerthana, K., Anukiruthika, T., Moses, J. A., & Anandharamakrishnan, C. (2020). Development of fiber-enriched 3D printed snacks from alternative foods: A study on button mushroom. *Journal of Food Engineering, 287*. https://doi.org/10.1016/j.jfoodeng.2020.110116

Lee, J. S., Oh, H., Choi, I., Yoon, C. S., & Han, J. (2022). Physico-chemical characteristics of rice protein-based novel textured vegetable proteins as meat analogues produced by low-moisture extrusion cooking technology. *LWT, 157*. https://doi.org/10.1016/j.lwt.2021.113056

Liu, Z., Bhandari, B., Prakash, S., Mantihal, S., & Zhang, M. (2019). Linking rheology and printability of a multicomponent gel system of carrageenan-xanthan-starch in extrusion based additive manufacturing. *Food Hydrocolloids, 87*, 413–424. https://doi.org/10.1016/j.foodhyd.2018.08.026

Liu, Z., Zhang, M., Bhandari, B., & Wang, Y. (2017). *3D printing: Printing precision and application in food sector* (Vol. 69,, 83–94. https://doi.org/10.1016/j.tifs.2017.08.018

Ozel, B., & Oztop, M. H. (2022). Rheology of food hydrogels, and organogels. In *Advances in Food Rheology and Its Applications: Development in Food Rheology, Second Edition* (pp. 661–688). Elsevier. 10.1016/B978-0-12-823983-4.00018-2.

Pérez, B., Nykvist, H., Brøgger, A. F., Larsen, M. B., & Falkeborg, M. F. (2019). Impact of macronutrients printability and 3D-printer parameters on 3D-food printing: A review. *Food Chemistry, 287*, 249–257. https://doi.org/10.1016/j.foodchem.2019.02.090

Phuhongsung, P., Zhang, M., & Devahastin, S. (2020). Investigation on 3D printing ability of soybean protein isolate gels and correlations with their rheological and textural properties via LF-NMR spectroscopic characteristics. *LWT, 122*. https://doi.org/10.1016/j.lwt.2020.109019

Phuhongsung, P., Zhang, M., Devahastin, S., & Mujumdar, A. S. (2022). Defects in 3D/4D food printing and their possible solutions: A comprehensive review. In *Comprehensive Reviews in Food Science and Food Safety* (Vol. 21, Issue 4, pp. 3455–3479). John Wiley and Sons Inc. 10.1111/1541-4337.12984.

Portanguen, S., Tournayre, P., Sicard, J., Astruc, T., & Mirade, P. S. (2021). 3D food printing: Genesis, trends and prospects. In *Future Foods: Global Trends, Opportunities, and Sustainability Challenges* (pp. 627–644). Elsevier. 10.1016/B978-0-323-91001-9.00008-6.

Qiu, Y., McClements, D. J., Chen, J., Li, C., Liu, C., & Dai, T. (2023). Construction of 3D printed meat analogs from plant-based proteins: Improving the printing performance of soy protein- and gluten-based pastes facilitated by rice protein. *Food Research International, 167*. https://doi.org/10.1016/j.foodres.2023.112635

R Core Team. (2022). *R: A Language and Environment for Statistical Computing.* https://www.R-project.org/.

Wang, D., Guo, J., Wang, Y., Yang, Y., Jiang, B., Li, D., … Liu, C. (2023). Whey protein isolate nanofibrils as emulsifying agent to improve printability of Cheddar cheese for 3D printing. *Food Hydrocolloids, 142.* https://doi.org/10.1016/j.foodhyd.2023.108807

Wang, L., Zhang, M., Bhandari, B., & Yang, C. (2018). Investigation on fish surimi gel as promising food material for 3D printing. *Journal of Food Engineering, 220*, 101–108. https://doi.org/10.1016/j.jfoodeng.2017.02.029

Wu, J. (2018). Study on optimization of 3D printing parameters. *IOP Conference Series: Materials Science and Engineering, 392*(6). https://doi.org/10.1088/1757-899X/392/6/062050

Yang, F., Zhang, M., & Bhandari, B. (2017). Recent development in 3D food printing. *Critical Reviews in Food Science and Nutrition, 57*(14), 3145–3153. https://doi.org/10.1080/10408398.2015.1094732

Yang, F., Zhang, M., Bhandari, B., & Liu, Y. (2018). Investigation on lemon juice gel as food material for 3D printing and optimization of printing parameters. *LWT, 87*, 67–76. https://doi.org/10.1016/j.lwt.2017.08.054

Zhang, J. Y., Pandya, J. K., McClements, D. J., Lu, J., & Kinchla, A. J. (2022). Advancements in 3D food printing: a comprehensive overview of properties and opportunities. In *Critical Reviews in Food Science and Nutrition* (Vol. 62, Issue 17, pp. 4752–4768). Taylor and Francis Ltd. 10.1080/10408398.2021.1878103.